THE JOURNAL OF PHYSICAL CHEMISTRY A

Article

pubs.acs.org/JPCA

Reaction of Hydroxyl Radicals with C_4H_5N (Pyrrole): Temperature and Pressure Dependent Rate Coefficients

Terry J. Dillon, Maria E. Tucceri,[†] Katrin Dulitz,[‡] Abraham Horowitz, Luc Vereecken, and John N. Crowley*

Division of Atmospheric Chemistry, Max-Planck-Institut für Chemie, 55020 Mainz, Germany

Supporting Information

ABSTRACT: Absolute (pulsed laser photolysis, 4−639 Torr N_2 or air, 240−357 K) and relative rate methods (50 and 760 Torr air, 296 K) were used to measure rate coefficients k_1 for the title reaction, OH + C_4H_5N → products (R1). Although the pressure and temperature dependent rate coefficient is adequately represented by a falloff parametrization, calculations of the potential energy surface indicate a complex reaction system with multiple reaction paths (addition only) in the falloff regime. At 298 K and 760 Torr (1 Torr = 1.33 mbar) the rate coefficient obtained from the parametrization is $k_1 = (1.28 \pm 0.1) \times 10^{-10}$ cm^3 molecule^{-1} s^{-1}, in good agreement with the value of $(1.10 \pm 0.27) \times 10^{-10}$ cm^3 molecule^{-1} s^{-1} obtained in the relative rate study (relative to C_5H_8, isoprene) at this temperature and pressure. The accuracy of the absolute rate coefficient determination was enhanced by online optical absorption measurements of the C_4H_5N concentration at 184.95 nm using a value $\sigma_{184.95nm} = (1.26 \pm 0.02) \times 10^{-17}$ cm^2 molecule^{-1}, which was determined in this work.

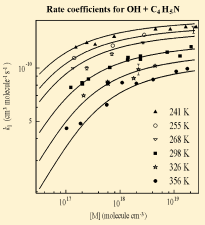

1. INTRODUCTION

Reactions with the hydroxyl radical (OH) define the lifetimes and abundance of various naturally occurring and anthropogenically emitted hydrocarbons. Aromatic and heterocyclic compounds are present in significant concentrations in the atmosphere and their reactions with the OH radical have been subject of numerous kinetic studies,[1,2] which indicate that two reaction pathways are possible; addition followed by subsequent product formation and/or direct abstraction. Although C_4H_5N, a nitrogen containing heterocyclic species with aromatic character, has not been measured in the atmosphere, it has recently been used as reference trace gas in a new instrument (comparative reactivity method, CRM) for measuring atmospheric OH lifetimes.[3] In brief, the CRM monitors the modulation in the concentration of C_4H_5N due to reaction with synthetically generated OH when either zero-air or real air are sampled. The derivation of OH reactivity using CRM requires accurate values for k_1. Given that the two published studies of the rate coefficient for reaction between C_4H_5N and OH (R1) were conducted some 25 years ago[4,5] and that these covered only a limited range of temperatures and pressures, a more detailed study is warranted. Exploring the dependence of k_1 on pressure and temperature would enable extension of the CRM to mobile platforms that demand operation at various ambient conditions.

$$OH + C_4H_5N \rightarrow \text{products} \qquad \text{(R1)}$$

In the present study, the technique of pulsed laser photolysis (PLP) radical generation, coupled to OH detection by laser induced fluorescence (LIF) was employed to determine absolute values of $k_1(T,P)$ at different pressures and temperatures as low as 241 K. Confidence in the accuracy of these results was enhanced by online optical absorption measurements of the pyrrole concentration, $[C_4H_5N]$. Therefore, the absorption cross-section (σ) for C_4H_5N at λ = 184.95 nm was determined. Furthermore, the relative rate method (with FTIR detection of reactants) was used to derive k_1 at 296 ± 2 K and at 50 and 760 Torr air. Interpretation of the experimental data set was aided by quantum chemical calculations.

2. METHODS

2.1. Pulsed Laser Photolysis with Laser Induced Fluorescence (PLP-LIF). The PLP-LIF techniques employed have been used in previous kinetic studies from this laboratory of reactions between volatile organic compounds and OH. Experimental details have been published previously,[6,7] and therefore, only a brief description is given here. Photolysis of H_2O_2 with an excimer laser operating at 248 nm was used to generate OH radicals (R2) in a 500 cm^3 temperature-controlled cell. Gas flow rates were chosen so that a fresh gas sample was available for photolysis at each laser pulse (10 Hz).

$$H_2O_2 + h\nu(248\ \text{nm}) \rightarrow 2OH \qquad \text{(R2)}$$

In a typical experiment, at a laser fluence of 10 mJ cm^{-2} and $[H_2O_2] = 1 \times 10^{14}$ molecules cm^{-3}, about 4×10^{11} molecules cm^{-3} of OH was generated. The OH radicals thus formed were then excited at 281.997 nm (the $A^2\Sigma$ (v = 1) ← $X^2\Pi$ (v = 0), Q_{11} (1) transition) by the output of a Nd:YAG pumped dye laser operating with Rhodamine 6G. OH fluorescence was detected by a photomultiplier tube (PMT) and recorded by a

Special Issue: A. R. Ravishankara Festschrift

Received: November 22, 2011
Revised: January 5, 2012
Published: January 20, 2012

   dx.doi.org/10.1021/jp211241x | J. Phys. Chem. A 2012, 116, 6051−6058

gated charge integrator. The detection limit, in the absence of C_4H_5N, was found to be $\approx 10^9$ molecules cm^{-3} for a S/N = 1 (20 scans).

2.2. Determination of Absorption Cross-Sections for C_4H_5N, $\sigma_{184.95nm}$. The accuracy of the rate coefficient determinations was improved by online measurements of $[C_4H_5N]$. A 43.8 cm long absorption cell, located downstream of the photolysis cell and equipped with a low-pressure Hg lamp and suitable filters, provided a means of direct online measurement of optical density at λ = 184.95 nm. The absorption cross-section of C_4H_5N at λ = 184.95 nm, $\sigma_{184.95nm}$, was derived in static experiments using a monochromator purged with N_2 to enable use of the 184.95 nm Hg line and a diode-array detector. Optical densities of C_4H_5N at 296 ± 2 K and pressure range of 1−3.5 Torr were determined in a 1 cm long cell or at lower pressures in a 30.4 cm cell. Concentrations of C_4H_5N were determined by pressure measurement using a calibrated capacitance manometer (MKS) and monitored continuously during each optical scan.

2.3. Relative Rate Experiments with FTIR. The rate constant of the reaction of OH with C_4H_5N relative to its reaction with C_5H_8 via (R3), k_1/k_3, was determined in a 44 L cylindrical quartz reactor cell fitted with internal multipath optics to give an effective optical path length of ∼30 m.[8]

$$OH + C_5H_8 \rightarrow (\text{products}) \quad (R3)$$

Experiments with two different sources of OH radicals were carried out. One group of experiments employed five Philips-TUV 40 W lamps (emitting mainly at 254 nm) mounted outside the reactor to generate OH by the photolysis of H_2O_2. Alternatively, OH radicals were produced by the photolysis of methyl nitrite in air using six Philips-TL12 40 W lamps (320−380 nm) via (R4)−(R6)

$$CH_3ONO + h\nu \rightarrow CH_3O + NO \quad (R4)$$

$$CH_3O + O_2 \rightarrow CH_2O + HO_2 \quad (R5)$$

$$HO_2 + NO \rightarrow OH + NO_2 \quad (R6)$$

Static mixtures of C_4H_5N (4.7−6.8) × 10^{13} molecules cm^{-3}, C_5H_8 (1.3−2.3) × 10^{14} molecules cm^{-3}, and H_2O_2 (or CH_3ONO and NO both at a concentration of (3.2−6.5) × 10^{14} molecules cm^{-3}) were prepared in the reactor. Approximate concentrations were determined manometrically. Finally, the mixture was topped with air to the desired pressure, 760 or 50 Torr, and then allowed to stand for 15−20 min to ensure mixing. Prior to, and at regular intervals after photolysis, the spectrum of the mixture (550−2500 cm^{-1}, 0.5 cm^{-1} resolution, typically 32 coadded scans) was recorded using a Bomem DA-008 spectrometer with a MCT detector. The variation of the C_4H_5N and C_5H_8 concentrations with photolysis duration was determined for different exposure times. The exposure times were always shorter than 170 s, and no change in the cell temperature was observed over this period. The relative change in the concentration of the two reactants was then derived by fitting the post photolysis spectra to the prephotolysis reference using absorption features at ∼720 cm^{-1} for C_4H_5N and ∼900 cm^{-1} for C_5H_8. The values thus obtained were then corrected for the reactant's removal by dark reactions (<1%) as well as direct photolysis (<4% for C_4H_5N only).

2.4. Chemicals. N_2 (Messer 99.999) and synthetic air (Messer, 20.5% O_2 in N_2) were used without further purification. NO (Aldrich, >98.5%) was purified by passing it through a silica column at −78 °C; C_4H_5N (Aldrich 98%+) and C_5H_8 (Aldrich, 99%) were degassed and purified by trap-to-trap distillations retaining the middle fraction. Their diluted mixtures in N_2 were stored in blackened glass bulbs. H_2O_2 (Peroxid-Chemie GmbH, ≈80 wt %) was concentrated to >90 wt % by evacuative removal of water. CH_3ONO was prepared[13] by dropwise addition of 50% H_2SO_4 (Roth, >99.5%) to a saturated solution of $NaNO_2$ (Aldrich 97%) and CH_3OH (Merck, 99.9%). A stream of He (Westfalen, 99.999%) carried the reaction products to a trap held at 195 K. The CH_3ONO was then degassed, vacuum distilled, and stored at 233 K under vacuum in the dark.

2.5. Quantum Chemical Calculations. The potential energy surface of the C_4H_5N + OH reaction was characterized by quantum chemical calculations. The geometries and vibrational characteristics of the critical points on the potential energy surface were obtained using the M05-2X/cc-pVTZ density functional theory,[9] as implemented in the Gaussian-09 program.[10] The zero-point energies were scaled by a factor of 0.964. The highest-level energy estimates for these geometries were calculated at the ROHF-CCSD(T)/aug-cc-pVTZ level of theory,[11] using the Molpro-2010.1 suite.[12] The geometries, vibrational frequencies, and energies of all intermediates and TS characterized on the PES are listed in Supporting Information. We were unable to obtain CCSD(T) energies for the prereactive complex due to convergence problems for the ROHF SCF wave function. As we aim here at a qualitative understanding of the reaction kinetics only, no RRKM-Master Equation analysis was done at this time.

3. RESULTS

3.1. Absorption Cross-Sections of C_4H_5N. $\sigma_{184.95nm}$ was determined using Beer−Lambert's law (E1)

$$OD = \ln(I_0/I) = \sigma_{184.95nm} l [C_4H_5N] \quad (E1)$$

where I_0 and I are the incident and transmitted light intensities, respectively, and l is the length of the optical path. Optical densities, OD, were measured at various pressures of C_4H_5N. The plot of the data according to (E1) is displayed in Figure 1.

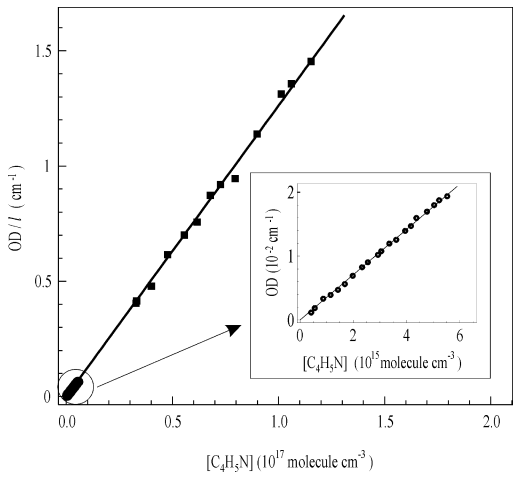

Figure 1. Beer−Lambert plot of optical density (per cm) observed at 184.95 nm vs concentration of C_4H_5N. A proportional fit to this data was used to determine $\sigma_{184.95}$ = (1.26 ± 0.02) × 10^{-17} cm^2 $molecule^{-1}$, as detailed in section 3.1. For clarity, the insert replots the results obtained in the 30.4 cm cell at low $[C_4H_5N]$.

dx.doi.org/10.1021/jp211241x | J. Phys. Chem. A 2012, 116, 6051−6058

A least-squares analysis yields $\sigma_{184.95nm} = (1.26 \pm 0.02) \times 10^{-17}$ cm^2 molecule^{-1}. The errors quoted are statistical only (two standard deviations). The main source of error in this determination is the loss of C_4H_5N (max of 5%) during the optical scans at pressures approaching its vapor pressure. The $[C_4H_5N]$ used for the determination of $\sigma_{184.95nm}$ according to (E1) was thus derived from the average between the initial and final pressures measured. We estimate the overall error of the $\sigma_{184.95nm}$ determination to be 5%. The cross-section thus obtained is ~50% larger than the single literature value of 8.38×10^{-18} cm^2 molecule^{-1} [13] reported for a similar wavelength (184.96 nm). The reason for this difference is unclear, though we note our study utilized a line source (low pressure Hg lamp), whereas the VUV spectrum of Palmer et al., 113−248 nm,[13] used a synchrotron source. Also, the focus of Palmer et al. was on spectroscopic assignment rather than absolute absorption cross-sections, which they did not report in their manuscript, but which were privately communicated to an online compendium of absorption spectra.[14] Later, we show that the rate coefficients obtained using this cross-section to calculate C_4H_5N concentrations are in agreement (15%) with those derived from relative rate studies that do not rely on absolute measurements of concentration. Thus we are confident that our C_4H_5N cross-section is accurate.

3.2. Absolute Values of k_1 Using PLP-LIF. The PLP-LIF studies were carried under pseudo-first-order conditions with quasi-instantaneous generation of OH (laser pulse width of <20 ns) and $[C_4H_5N] \gg [OH]$, such that the OH time profiles were described by

$$[OH]_t = [OH]_0 \exp(-Bt) \quad \text{(E2)}$$

where $[OH]_t$ is the OH concentration (molecules cm^{-3}) at time t after the laser pulse. $B = k_1[C_4H_5N] + d$ is the pseudo-first-order rate coefficient for OH-loss, which includes a term d (s^{-1}) that accounts for both nonreactive OH-losses due to transport of OH out of the reaction zone and reaction of OH with the precursor H_2O_2 (R7).

$$OH + H_2O_2 \rightarrow HO_2 + H_2O \quad \text{(R7)}$$

The use of low [OH] and hence low conversion of C_4H_5N assures that secondary loss of OH, e.g., by its self-reaction or reaction with products can be disregarded fully. This was verified by noting no change in B with variation of the laser fluence (and thus the initial OH concentration) by a factor of 5. Figure 2 displays typical OH decay profiles recorded in the presence of three different C_4H_5N concentrations, while other conditions (P = 74.4 Torr (N_2), T = 298 K, and $[H_2O_2] \approx 1 \times 10^{14}$ molecules cm^{-3}) remained constant. At all temperatures and pressures, the OH decays were exponential over at least 2 orders of magnitude so that fitting the data with expression (E2) yields precise values of B with statistical errors generally less than ±2%.

The desired rate constant k_1 was derived from linear, weighted least-squares fitting of B versus $[C_4H_5N]$ as shown in representative data sets of Figure 3. The rate coefficients obtained at this pressure are $k_1(255\ K) = (1.44 \pm 0.04) \times 10^{-10}$ cm^3 molecule^{-1} s^{-1}, $k_1(298\ K) = (1.18 \pm 0.01) \times 10^{-10}$ cm^3 molecule^{-1} s^{-1}, and $k_1(356\ K) = (0.80 \pm 0.04) \times 10^{-10}$ cm^3 molecule^{-1} s^{-1}, indicating a significant temperature dependence of k_1. The intercept, $d \sim 200$ s^{-1}, is consistent with known diffusive loss rates in this apparatus at this pressure and the rate coefficient for reaction (R7). A summary of the complete data set of k_1 determinations at various temperatures (240−357 K) and pressures (4−639 Torr) of both N_2 and air is presented in Table 1. As discussed later, k_1 was found to depend both on temperature and on pressure in a manner broadly consistent with a termolecular process involving formation and collisional stabilization of an energized association complex.

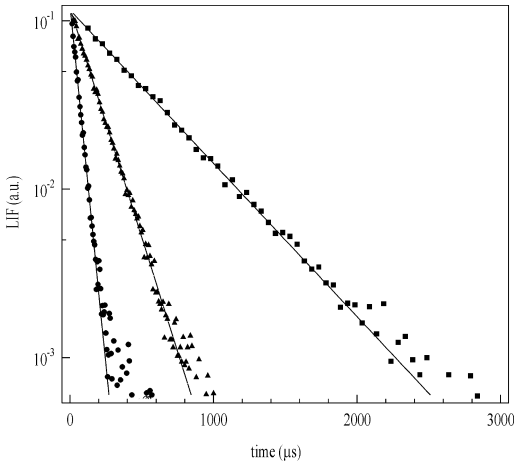

Figure 2. Plot of time-resolved OH LIF signal recorded in the presence of C_4H_5N. Initial $[OH] \approx 1 \times 10^{11}$ molecules cm^{-3}, T = 298 K and P = 75 Torr (N_2). Data were fit with expression (E2) to yield pseudo-first-order rate coefficients (B). Upper curve: $[C_4H_5N] = 2.4 \times 10^{13}$ molecules cm^{-3}, B = 2097 ± 26 s^{-1}. Middle curve: $[C_4H_5N] = 7.4 \times 10^{13}$ molecules cm^{-3}, B = 6271 ± 92 s^{-1}. Lower curve: $[C_4H_5N] = 2.39 \times 10^{14}$ molecules cm^{-3}, B = 19654 ± 368 s^{-1}.

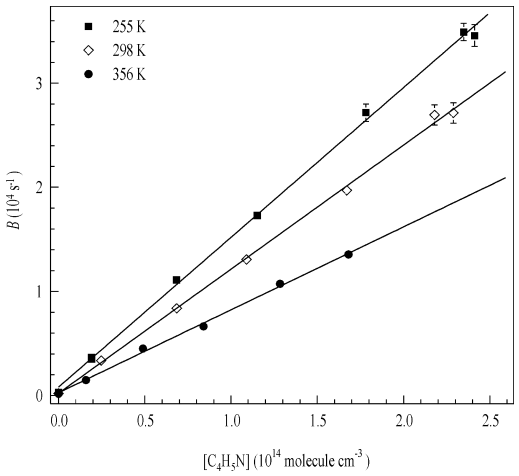

Figure 3. Plots of B vs $[C_4H_5N]$, used to determine k_1 (see expression E2). Unweighted linear fits to this data yield (in units of 10^{-10} cm^3 molecule^{-1} s^{-1}): $k_1(255\ K) = 1.44 \pm 0.04$, $k_1(298\ K) = 1.18 \pm 0.01$, and $k_1(356\ K) = 0.80 \pm 0.04$.

3.3. RR-FTIR Determination of k_1/k_3. Expression (E3), where k_1 and k_3 refer to the reaction of OH with C_4H_5N and C_5H_8, respectively, was used in the derivation of k_1/k_3 in air (50 and 760 Torr and 296 ± 2 K).

$$\ln([C_4H_5N]_0/[C_4H_5N]) = (k_1/k_3) \ln([C_5H_8]_0/[C_5H_8]) \quad \text{(E3)}$$

The infrared absorption regions used to derive changes in concentration (depletion factors) of C_4H_5N and C_5H_8 are displayed in Figure 4. The depletion factor was obtained by least-squares fitting of the postphotolysis spectrum to that obtained prior to photolysis over the identical spectral range.

dx.doi.org/10.1021/jp211241x | J. Phys. Chem. A 2012, 116, 6051−6058

Table 1. Summary of the Results of the PLP-LIF Determination of k_1

T (K)	P (Torr)	k_1[a]
241 ± 1	3.80	1.31 ± 0.02
	6.08	1.39 ± 0.01
	8.65	1.36 ± 0.02
	19.5	1.51 ± 0.02
	112.8	1.66 ± 0.01
	210.8	1.66 ± 0.02
	410.8	1.71 ± 0.03
	639.0	1.71 ± 0.03
255 ± 1	3.75	1.14 ± 0.01
	19.4	1.34 ± 0.01
	74.0	1.54 ± 0.02
268 ± 1	3.75	1.00 ± 0.01
	6.70	0.997 ± 0.02
	19.5	1.20 ± 0.02
	74.0	1.39 ± 0.02
	635.0	1.71 ± 0.14
298 ± 1	3.80	0.778 ± 0.01
	6.20 (air)	0.811 ± 0.01
	6.10	0.827 ± 0.008
	8.10	0.866 ± 0.008
	20.0	1.01 ± 0.01
	42.8	1.11 ± 0.01
	43.3 (air)	1.15 ± 0.01
	74.4	1.16 ± 0.001
	74.0	1.15 ± 0.02
	74.0	1.12 ± 0.01
	74.0 (air)	1.17 ± 0.00
	230.0	1.23 ± 0.01
	396.0	1.17 ± 0.02
	637.0	1.32 ± 0.03
326 ± 1	7.1	0.700 ± 0.008
	20.0 (air)	0.824 ± 0.005
	20.0 (air)	0.837 ± 0.003
	20.3	0.813 ± 0.003
	60.3	0.876 ± 0.003
	74.0	0.984 ± 0.07
	149.9	1.03 ± 0.004
356 ± 2	3.80	0.457 ± 0.17
	6.90	0.486 ± 0.007
	21.0	0.620 ± 0.01
	39.9	0.827 ± 0.028
	74.0	0.819 ± 0.009
	150.7	0.861 ± 0.003
	396.0	0.958 ± 0.013
	637.0	0.992 ± 0.024

[a]Units are 10^{-10} cm^3 molecule^{-1} s^{-1}.

The residuals in Figure 4 are statistically scattered about zero, showing that no significant absorption by products of the C_4H_5N or C_5H_8 degradation was encountered in these spectral windows.

The data obtained when H_2O_2 is used as the OH source are shown in Figure 5 (upper panel) and yield values of k_1/k_3 = 1.03 ± 0.04 at 760 Torr and k_1/k_3 = 0.88 ± 0.04 at 50 Torr air. The errors quoted are 2 standard deviation, statistical uncertainty. The relative rate constants can be placed on an absolute basis using the evaluated, pressure independent rate coefficient for OH with C_5H_8 of 1.0×10^{-10} cm^3 molecule^{-1} s^{-1}, with an estimated error of 25%.[15] The result is $k_1 = (1.03 \pm 0.26) \times 10^{-10}$ at 760 Torr and $k_1 = (0.88 \pm 0.22) \times 10^{-10}$ cm^3 molecule^{-1} s^{-1} at 50 Torr, indicating a weak, but measurable pressure dependence of k_1 at 298 K. Figure 5 (lower panel) displays data

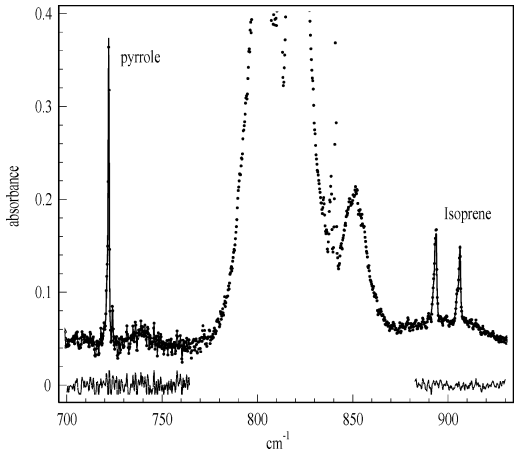

Figure 4. FTIR spectrum obtained after 45 s photolysis of a mixture containing CH_3ONO, NO, C_5H_8, and C_4H_5N. The solid lines are scaled reference spectra (obtained before photolysis) with the depletion factor obtained by least-squares fitting. The gray lines (around zero absorbance) are the fit residuals and also indicate the spectral windows used for analysis of C_5H_8 and C_4H_5N.

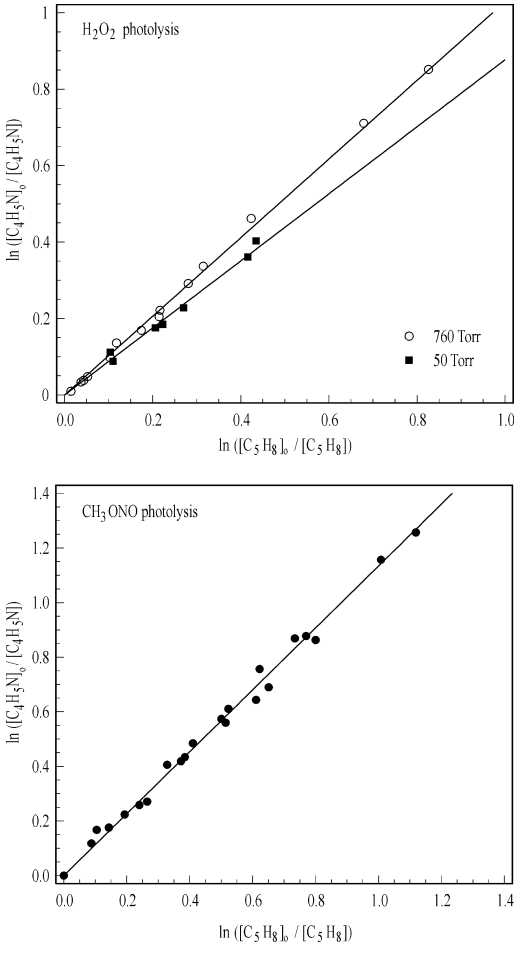

Figure 5. Upper panel: Relative rate plot for k_1/k_3 in air at 760 and 50 Torr and at 298 ± 2 K using H_2O_2 photolysis to generate OH. Lower panel: Relative rate plot for k_1/k_3 in air at 760 Torr and 298 ± 2 K using CH_3ONO photolysis to generate OH.

dx.doi.org/10.1021/jp211241x | J. Phys. Chem. A 2012, 116, 6051−6058

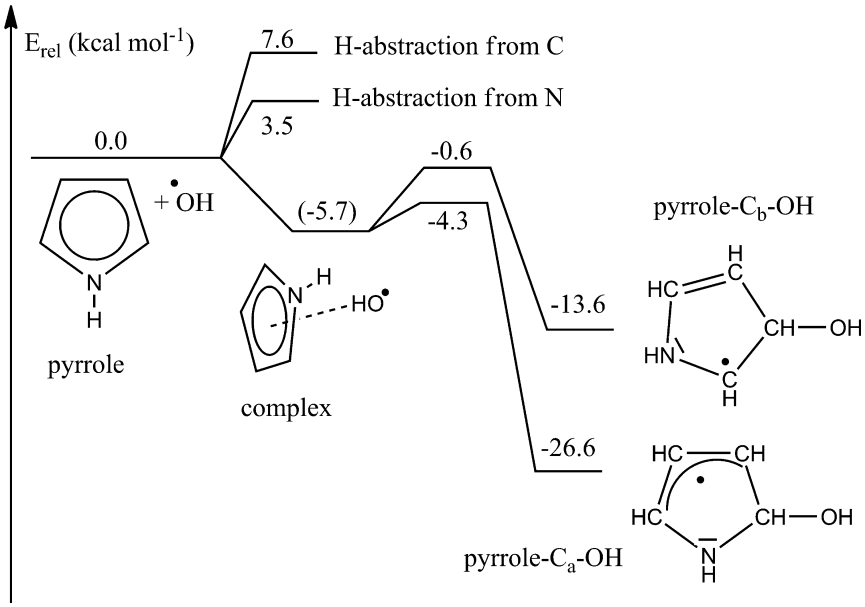

Figure 6. ZPE-corrected potential energy surface of the C_4H_5N + OH reaction at the ROHF-CCSD(T)/aug-cc-pVTZ//M05-2X/cc-pVTZ level of theory. Values in brackets are at the M05-2X/cc-pVTZ level of theory.

obtained using CH_3ONO as OH source. In this case, a slightly larger rate coefficient ratio was obtained with k_1/k_3 value of 1.12 ± 0.03.

Differences in relative rates coefficients found when two distinct OH sources are used are often ascribed to the presence of extra removal pathways in one of the chemical systems. In both reaction systems, the only other radical present is HO_2 formed from OH + H_2O_2 (R7) and photolysis of CH_3ONO in the presence of air (R5) and (R6). The presence of NO in the CH_3ONO photolysis system should reduce the HO_2/OH ratio greatly in favor of OH ruling out a contribution to C_4H_5N-loss by reaction with HO_2 in this system. As the generation of OH via the photolysis of CH_3ONO also resulted in the larger relative rate coefficient, we can rule out HO_2 related effects. Alternatively, the presence of NO could conceivably accelerate the overall loss of C_4H_5N by preventing redissociation to reactants of a peroxy radical product. Evidence for this is, however, weak (see section 4.3), and in the absence of a definitive explanation for the (apparent) differences in relative rate coefficient obtained in the absence and presence of NO, and given that these differences are in any case rather small (9%), we combine all the relative rate results at 760 Torr to derive k_1/k_3 = 1.10 ± 0.03 and thus k_1 = (1.10 ± 0.27) × 10^{-10} cm^3 $molecule^{-1}$ s^{-1}.

3.4. Reaction Mechanism. The potential energy surface (PES) of the C_4H_5N + OH reaction is depicted in Figure 6. Two reaction types need to be considered: H-abstraction and OH-addition on the ring structure. The bond dissociation energies calculated for H-loss from the carbons (117−118 kcal mol^{-1}) and the nitrogen atom (92.6 kcal mol^{-1}) are in fair agreement with earlier theoretical work based on isodesmic reactions, at the CBS-APNO level of theory, by da Silva et al.[16] The hydrogen atom abstraction reactions were all found to proceed with a sizable barrier, ≥3 kcal mol^{-1}. For H-abstraction from the carbon atoms, this is not surprising, as it is an endothermic process by 1.4−1.8 kcal mol^{-1}, depending on the substrate carbon. The comparatively high barrier for the exothermic H-abstraction from the N-atom finds its origin in the changes in the π-system of the ring following H-loss. In C_4H_5N, the sp^2 hybridized N-atom has a lone pair in its p-orbital, conjugated with the double bonds of the carbon atoms and leading to a six-electron, five-membered aromatic structure; in pyrrol-*N*-yl, on the other hand, the lone pair on the nitrogen atom is located in the sp^2-orbital in the plane of the molecule, with the unpaired electron delocalized across the ring π-system but mostly across the two carbons adjacent to the nitrogen atom. The transition state for H-abstraction from the N-atom is then influenced by these very distinct wave functions, but not reaping the full stabilizing effect of either of them, leading to a higher energy barrier. We were unable to find an H-abstraction channel forming pyrrol-*N*-yl + H_2O proceeding through an addition−elimination mechanism, neither following addition on the N-atom (as suggested earlier in the literature[4,17]) nor following addition on the carbon atoms adjacent to the N-atom. H-abstraction also does not benefit from prereactive complex formation as described below, as the OH radical is positioned near the plane of the C_4H_5N molecule and points outward to obtain a suitable TS geometry.

The addition reaction of OH on the C_4H_5N ring proceeds through a prereactive complex where the OH radical forms a hydrogen bond of approximately 2.3 Å with the aromatic π-system, slightly off-center toward the carbon side of C_4H_5N. From this complex, two transition states were characterized for OH-addition on the C_4H_5N ring, one for each type of carbon atom. The most favorable addition is on the carbons adjacent to the N-atom, called C_a henceforth, leading to delocalization of the unpaired electron across the three remaining carbon atoms. Addition on the carbons furthest away from the nitrogen atom, labeled C_b from here on, leads to a product radical with the unpaired electron mostly located on a single carbon, with only minimal delocalization across the π-system; this lack of delocalization leads to a higher relative energy, and concomitantly a higher barrier for addition. Nonetheless, both addition channels have a barrier below the energy of the separated adduct. The addition on the C_a carbons is entropically slightly more favorable, as it has a somewhat earlier transition state with a C−O forming bond of length 2.17 Å, compared to addition to C_b with a separation of 1.98 Å. We

dx.doi.org/10.1021/jp211241x | J. Phys. Chem. A 2012, 116, 6051−6058

were unable to locate a stable adduct for addition of OH to the nitrogen atom and concluded that it is not a stable radical. Indeed, such an adduct with four bonds on the nitrogen atom would require a zwitterionic structure with a positively charged N-atom, and a negative charge and an unpaired electron to be placed across the ring. Combined with a loss of aromaticity, this implies an energy well above the C_4H_5N--HO complex or separated reactants.

4. DISCUSSION

4.1. Parameterization of the Absolute Rate Coefficients. Our results indicate that the reaction of OH with C_4H_5N is both temperature and pressure dependent with the same absolute rate coefficients obtained in nitrogen and air bath gases. The observation of a positive dependence on pressure and negative dependence on temperature is consistent with the results of the calculations of the PES and with previous studies on the reactions of OH with aromatic and heterocyclic compounds.[2,1,18−21]

The falloff of the observed rate constant k_1 with decreasing pressure can be attributed to the reversible formation of an excited complex or adduct, thus allowing the analysis and characterization of the falloff behavior using the widely adopted Troe formalism.[22−24]

$$k_1 = k_0[\mathrm{M}]/(1 + k_0[\mathrm{M}]/k_\infty)F \qquad \text{(E4)}$$

k_0 denotes the rate coefficients at the low-pressure limit and k_∞ stands for the high-pressure limiting value. Given the narrow temperature range, around 298 K covered here, the temperature dependence of the rate constants in (E4) is assumed to be given by $k_0 = k_0^{298}(T/298)^{n_0}$ and $k_\infty = k_\infty^{298}(T/298)^{n_\infty}$, where n_0 and n_∞ are the power coefficients. F is the broadening factor that, at moderate temperatures, is approximately given by

$$\log F \approx \log F_C/\{1 + [\log(k_0[\mathrm{M}]/k_\infty)/N)]^2\} \qquad \text{(E5)}$$

and

$$N = 0.75 - 1.27 \log F_C \qquad \text{(E6)}$$

The center broadening factor, F_C was estimated as described by Cobos and Troe.[25] Based on a total number of external rotational degrees of freedom of C_4H_5N and OH of 5, and a collision effeiciency of 0.3 for N_2, a value of $F_C = 0.39$ was obtained.[26]

A global, least-squares fit of k_1 to eq E4 was performed with four unconstrained variable parameters k_0^{298}, k_∞^{298}, n_0, and n_∞. The results are displayed as the solid lines in Figure 7. This falloff parametrization reproduces the pressure and temperature rate coefficient adequately and returns values of $k_0 = (1.07 \pm 0.04) \times 10^{-26}(T/298)^{-7.0\pm0.3}$ cm^6 molecule^{-2} s^{-1} and $k_\infty = (1.45 \pm 0.01) \times 10^{-10}$ $(T/298)^{1.40\pm0.04}$ cm^3 molecule^{-1} s^{-1}. Given that our quantum chemical calculations indicate that the reaction proceeds via multiple addition channels, this analysis is not rigorous and the values of k_0, k_∞, n_0, and n_∞ obtained should not be over-interpreted or used to extrapolate beyond the temperature and pressure regime of the experimental data. Rather, they represent a set of parameters that reproduce the measured values of k_1 within a well-known framework for pressure dependent reactions in the falloff regime. Bearing this in mind, we note that the (two) values of k_1 obtained at the lowest pressures in the data sets at 326 and 356 lie slightly above that predicted by the parametrization and that the temperature dependence of the low-pressure rate coefficient is rather large ($n_0 = -7.0 \pm 0.3$) and that of the high-pressure rate constant is slightly positive ($n_\infty = 1.4$). Such observations are consistent with (but cannot be considered proof of) the presence of multiple reaction pathways with different falloff behavior.

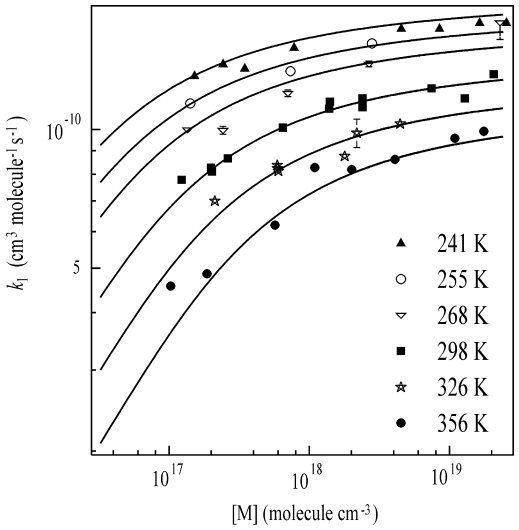

Figure 7. Pressure and temperature dependent values of k_1 for the absolute (PLP-LIF) studies. The solid lines are fit to the standard Troe expression (E4).

4.2. Comparison between the PLP-LIF and Relative Rate FTIR Determinations of k_1. Extrapolation of the PLP-LIF data set using the parametrization listed above results in a value of $k_1 = (1.28 \pm 0.1) \times 10^{-10}$ cm^3 molecule^{-1} s^{-1} at 298 K and 760 Torr (errors include an estimate of systematic error due to, e.g., errors in the C_4H_5N cross-section at 184.95 nm). This result is in reasonable agreement with our relative rate determination of $k_1 = (1.10 \pm 0.27) \times 10^{-10}$ cm^3 molecule^{-1} s^{-1}. The corresponding value of k_1 at 298 K and 50 Torr is 1.12×10^{-10} cm^3 molecule^{-1} s^{-1}, i.e., an increase of 14% going from 50 to 760 Torr. This is consistent with the increase in rate coefficient of 17 ± 10% derived from the relative studies at 50 and 760 Torr using H_2O_2 as the OH source.

4.3. Comparison with Literature. There have been three previous determinations (two absolute, one relative) of the rate coefficient, k_1, and these results are summarized in Figure 8 along with our parametrization above. Atkinson et al.[4] conducted a relative rate study of k_1 at 295 K and in 750 Torr of air. They also used CH_3ONO as the OH precursor but used C_3H_6 (propene) rather than C_5H_8 as the reference reactant (both reactants detected by GC-FID) to derive $k_1/k_8 = 4.55 \pm 0.13$.

$$\mathrm{OH} + \mathrm{C_3H_6} \rightarrow \text{products} \qquad \text{(R8)}$$

Use of the preferred values[15] of $k_8 = (2.9 \pm 0.73) \times 10^{-11}$ cm^3 molecule^{-1} s^{-1} at 760 Torr and 295 K results in $k_1 = (1.32 \pm 0.33) \times 10^{-10}$ cm^3 molecule^{-1} s^{-1}, which is >20% larger than our value derived relative to C_5H_8. In this regard, we note that relative rate coefficients are best derived using reactant pairs that have similar rate coefficients, which may indicate that C_3H_6 was not the ideal reference reactant for study of the C_4H_5N + OH reaction. We also note that, using the same technique, Atkinson and co-workers[27] have derived a relative rate coefficient for the reactant pair C_5H_8/C_3H_6 of $k_3/k_8 = 3.81 \pm 0.17$, which, when combined with their value $k_1/k_8 = 4.55 \pm 0.13$, results in $k_1/k_3 = 1.19 \pm 0.06$. Within

dx.doi.org/10.1021/jp211241x | J. Phys. Chem. A 2012, 116, 6051−6058

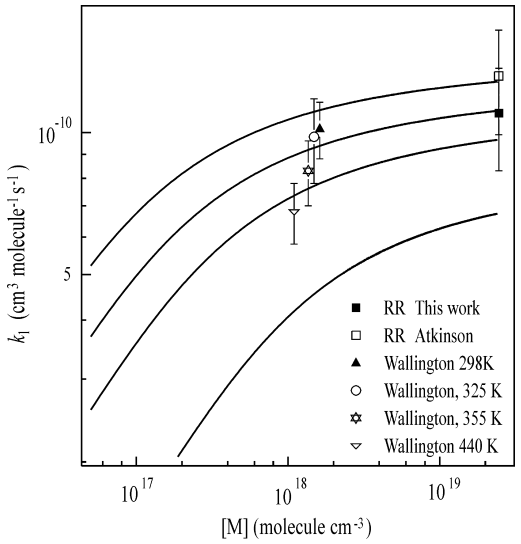

Figure 8. Comparison with literature results. The solid lines are the parametrization from the PLP-LIF study of k_1 in N_2 and air. The data set of Wallington[5] (obtained in Ar) has not been corrected for third-body quenching efficiency relative to N_2. RR = relative rate study. Atkinson = ref 4.

combined uncertainties, this is consistent with our direct determination of the relative reactivity of C_4H_5N to C_5H_8 of $k_1/k_3 = 1.10 \pm 0.03$.

Wallington[5] used a flash photolysis, resonance fluorescence technique to study the temperature dependence (298−440 K) and pressure dependence (25−100 Torr Ar) of k_1. As in the present study, the rate coefficient was found to increase with decreasing temperature, though, within experimental scatter, no dependence on pressure at 298 K was observed and Wallington reported $k_1 = 2.7^{+0.8}_{-0.6} \times 10^{-11} \exp[(403 \pm 93)/T]$ cm^3 molecule^{-1} s^{-1}. Wallington reports individual values of k_1 of $(1.05 \pm 0.06) \times 10^{-10}$, $(1.02 \pm 0.14) \times 10^{-10}$, and $(1.03 \pm 0.22) \times 10^{-10}$ cm^3 molecule^{-1} s^{-1} at 25, 50, and 100 Torr of Ar at 298 K. Inspection of these data suggests that their precision was not adequate to detect the small trend in k_1 (<20%) expected over this small pressure range at 298 K. The temperature dependent data of Wallington (all at 50 Torr Ar) are plotted in Figure 8. For this comparison we ignore differences in third body quenching efficiency between N_2, air, and Ar. The trend in k_1 seen by Wallington is broadly consistent with that measured in the present study and the three lowest-temperature data points agree within the error bars with our parametrized rate coefficient at the same temperatures. The exception to this is the data point of Wallington at 440 K, which, at $(6.8 \pm 1.0) \times 10^{-11}$ cm^3 molecule^{-1} s^{-1}, is significantly larger than the value predicted by our parametrization. In general, the data of Wallington suggest a weaker temperature dependence at pressures close to 50 Torr than we derived. However, extrapolation of our parametrization to 440 K without fully understanding the mechanism of the reaction should be regarded as precarious. In a review article of OH reactions with organic trace gases, Atkinson[17] summarizes the results of a further kinetic study[28,29] of (R1) using the flash-photolysis, resonance fluorescence method. Consistent with the present study, Witte and Zetzsch[28] report that the rate coefficient increased with pressure and displayed a negative dependence on temperature from 298 to 442 K with biexponential behavior at 392 K and above. This data set is presently subject (C. Zetzsch, personal communication) to a rigorous reanalysis using improved software tools to extract kinetic parameters from the observed biexponential OH decays.[30]

4.4. Mechanistic Interpretation. The theoretical calculations indicate that, at the temperatures investigated, the C_4H_5N + OH reaction occurs exclusively by complex formation and addition: given the predicted energy barriers the contribution of H-abstraction, even at 356 K, is below 1%. A negative temperature dependence has been reported for many OH−alkene addition reactions, in particular the C_5H_8 + OH reactions, which proceed over a very similar potential energy surface with a prereactive complex and two energetically rather different addition TS. As has been discussed in great detail,[31,32] the negative T dependence is the result of both the barrierless complex formation and the submerged TS for addition. At the temperature range considered in this work, one should refrain from predicting the rate coefficient from either of these reaction steps separately, or from a canonical combination of them: flux calculations in master equation analyses at the E,J-resolved level are necessary to fully capture the temperature and pressure dependence of such systems.

Even at the highest pressures considered in this study, 639 Torr, it seems unlikely that the entire multistep reaction system proceeds in a high-pressure regime. In particular, the shallow energy well for the prereactive complex, and the very low exit channel barrier for addition on the C_a carbons will lead to deviations from a pure Maxwell−Boltzmann thermal energy distribution for this complex. As seen in Figure 7, though, the overall rate coefficient is already nearing its high-pressure limit at these pressures, especially at the lowest of temperatures. This indicates that the ratio of redissociation versus formation of complex and/or adducts is nearing its thermal ratio in these conditions within experimental accuracy. For a high-pressure, equilibrium Maxwell−Boltzmann energy distribution of the complex population, the dominant fate of the complex is OH-addition on carbon C_a, with a rate coefficient $>4 \times 10^{10}$ s^{-1} even at 250 K, and outrunning addition on the C_b carbons and redissociation by a factor of 2×10^3 (250 K) to 2×10^2 (350 K). At the higher, nascent energies directly after formation of the complex from C_4H_5N + OH, the contribution of addition onto the C_b carbons will be increased compared to this, especially at higher temperatures. Obviously, this is also the case for redissociation of the complex to C_4H_5N + OH; this competition leads to the observed pressure dependence.

The fate of the adducts, once formed, depends on the reaction conditions. At their nascent energies, they can redissociate back to the complex. This process occurs in competition with thermalization of the adducts in collisions with the bath gas. In air, the radical adducts are expected to react with O_2, and considering that air as a bath gas consists of 20% O_2, this could also include a contribution of (partially) chemically activated adducts. For resonance-stabilized OH-adducts, such as those formed from C_5H_8, it has been shown[33] that the peroxy radical adduct formed after O_2 addition on the OH-adduct can itself redissociate. This (pressure-dependent) redissociation, in turn, occurs in competition with bimolecular reactions of the peroxy radicals, e.g., with NO, HO_2, or RO_2. To further complicate matters, the well depths for OH-addition on C_4H_5N (Figure 6) are comparatively shallow. For comparison, the C_5H_8−OH adducts have stabilization energies of 35 and 24 kcal mol^{-1}, for resonance-stabilized or non-resonance-stabilized adducts, respectively, relative to the free reactants. For the C_4H_5N-C_a−OH adduct, high-pressure thermal redissociation to the

dx.doi.org/10.1021/jp211241x | J. Phys. Chem. A 2012, 116, 6051−6058

C_4H_5N−OH complex is then predicted to proceed at a rate of 1×10^{-6} s^{-1} (250 K) to 0.6 s^{-1} (350 K), whereas for the less stable C_4H_5N-C_b−OH adduct, predicted dissociation rates range from 23 s^{-1} (250 K) to 5×10^4 s^{-1} (350 K).

An in-depth treatment of the temperature and pressure dependence of the $C_4H_5N/OH/O_2/NO$ reaction system would need to consider all these competing reactions. At this time, the application of C_4H_5N as a reference trace gas in reactivity measurements does not warrant such a complex undertaking. The trends of the rate coefficient measured in this work is fully consistent with the mechanism presented here; the temperature and pressure ranges considered, however, are not wide enough to irrefutably distinguish between different mechanisms, or to help calibrate all critical parameters in the theoretical kinetic model.

5. CONCLUSIONS

We have measured absolute rate coefficients for the reaction of OH with C_4H_5N and identified a positive dependence on pressure and a negative dependence on temperature. The experimental data can be described by low-pressure and high-pressure rate coefficients within a falloff parametrization. Relative rate studies confirmed both the magnitude of the rate coefficient at 760 Torr pressure and room temperature and also the effect of pressure. Our theoretical calculations of the potential energy surface indicate formation of a prereaction complex with multiple addition pathways, but no possibility of direct abstraction. Our rate coefficients enable application of the comparative reactivity technique at pressures other than 760 Torr and 298 K.

■ ASSOCIATED CONTENT

Supporting Information

The geometries, vibrational frequencies, and energies of all intermediates and transition states characterized on the PES. This information is available free of charge via the Internet at http://pubs.acs.org.

■ AUTHOR INFORMATION

Corresponding Author

*E-mail: john.crowley@mpic.de.

Present Addresses

[†]Instituto de Investigaciones Fisicoquímicas Teóricas y Aplicadas (INIFTA), Departamento de Química, Facultad de Ciencias Exactas, Universidad Nacional de La Plata, cc. Sixteen suc. 4, 1900 La Plata, Argentina.

[‡]Physical & Theoretical Chemistry Laboratory, University of Oxford, Oxford OX1 3QZ, United Kingdom.

■ ACKNOWLEDGMENTS

We gratefully acknowledge financial support from the MPI. M.E.T. thanks CONICET for support.

■ REFERENCES

(1) Atkinson, R.; Arey, J. *Chem. Rev.* **2003**, *103*, 4605−4638.

(2) Calvert, J. G.; Atkinson, R.; Becker, K. H.; Seinfeld, J. H.; Wallington, T. J.; Yarwood, G. *The mechanism of atmospheric oxidation of aromatic hydrocarbons*; Oxford University Press: New York, 2002.

(3) Sinha, V.; Williams, J.; Crowley, J. N.; Lelieveld, J. *Atmos. Chem. Phys.* **2008**, *8*, 2213−2227.

(4) Atkinson, R.; Aschmann, S. M.; Winer, A. M.; Carter, W. P. L. *Atmos. Environ.* **1984**, *18*, 2105−2107.

(5) Wallington, T. J. *Int. J. Chem. Kinet.* **1986**, *18*, 487−496.

(6) Wollenhaupt, M.; Carl, S. A.; Horowitz, A.; Crowley, J. N. *J. Phys. Chem.* **2000**, *104*, 2695−2705.

(7) Dillon, T. J.; Hölscher, D.; Sivakumaran, V.; Horowitz, A.; Crowley, J. N. *Phys. Chem. Chem. Phys.* **2005**, *7*, 349−355.

(8) Raber, W. H.; Moortgat, G. K. Photooxidation of selected carbonyl compounds in air. In *Problems and Progress in Atmospheric Chemistry*; Barker, J. R., Ed.; World Scientific Publishing Co. Pte. Ltd.: Singapore, 2000.

(9) Zhao, Y.; Schultz, N. E.; Truhlar, D. G. *J. Chem. Theory Comput.* **2006**, *2*, 364−382.

(10) Frisch, M. J. et al. *Gaussian 03* (version C.01); Gaussian Inc.: Wallingford, CT, 2004.

(11) Knowles, P. J.; Hampel, C.; Werner, H.-J. *J. Chem. Phys.* **1993**, *99*, 5219−5227.

(12) Werner, H.-J.et al. *MOLPRO*, version 2010.1, a package of ab initio programs, 2010.

(13) Palmer, M. H.; Walker, I. C.; Guest, M. F. *Chem. Phys.* **1998**, *238*, 179−199.

(14) Keller-Rudek, H.; Moortgat, G. K. *MPI-Mainz-UV-VIS Spectral Atlas of Gaseous Molecules*, www.atmosphere.mpg.de/spectral-atlas-mainz.

(15) Atkinson, R.; Baulch, D. L.; Cox, R. A.; Crowley, J. N.; Hampson, R. F.; Hynes, R. G.; Jenkin, M. E.; Rossi, M. J.; Troe, J. *Atmos. Chem. Phys.* **2006**, 3625−4055.

(16) da Silva, G.; Moore, E. E.; Bozzelli, J. W. *J. Phys. Chem. A* **2006**, *110*, 13979−13988.

(17) Atkinson, R. *J. Phys. Chem. Ref. Data* **1989**, *Monograph 1*, 1−246.

(18) Bohn, B.; Zetzsch, C. *Phys. Chem. Chem. Phys.* **1999**, *1*, 5097−5107.

(19) Bohn, B. *J. Phys. Chem. A* **2001**, *105*, 6092−6101.

(20) Johnson, D.; Raoult, S.; Rayez, M. T.; Rayez, J. C.; Lesclaux, R. *Phys. Chem. Chem. Phys.* **2002**, *4*, 4678−4686.

(21) Noda, J.; Volkamer, R.; Molina, M. J. *J. Phys. Chem. A* **2009**, *113*, 9658−9666.

(22) Troe, J. *J. Phys. Chem.* **1979**, *83*, 114−126.

(23) Troe, J. *Ber. Bunsen-Ges. Phys. Chem. Chem. Phys.* **1983**, *87*, 161−169.

(24) Gilbert, R. G.; Luther, K.; Troe, J. *Ber. Bunsen-Ges. Phys. Chem. Chem. Phys.* **1983**, *87*, 169−177.

(25) Cobos, C. J.; Troe, J. *Z. Phys. Chem.* **2003**, *217*, 1031−1044.

(26) Atkinson, R.; Baulch, D. L.; Cox, R. A.; Crowley, J. N.; Hampson, R. F.; Hynes, R. G.; Jenkin, M. E.; Rossi, M. J.; Troe, J. *Atmos. Chem. Phys.* **2004**, *4*, 1461−1738.

(27) Atkinson, R.; Aschmann, S. M.; Winer, A. M.; Pitts, J. N. *Int. J. Chem. Kinet.* **1982**, *14*, 507−516.

(28) Witte, F.; Zetzsch, C. *9th International Symposium on Gas Kinetics*, Bordeaux, France; NOAA: Boulder, CO, 1986.

(29) Witte, F. Untersuchung der Temperaturabhängigkeit der Reaktion von OH-Radikalen mit heterocyclischen aromatischen Verbindungen. *Ph.D. thesis*, Universität Bochum, 1987.

(30) Koch, R.; Knispel, R.; Elend, M.; Siese, M.; Zetzsch, C. *Atmos. Chem. Phys.* **2007**, *7*, 2057−2071.

(31) Greenwald, E. E.; North, S. W.; Georgievskii, Y.; Klippenstein, S. J. *J. Phys. Chem. A* **2005**, *109*, 6031−6044.

(32) Greenwald, E. E.; North, S. W.; Georgievskii, Y.; Klippenstein, S. J. *J. Phys. Chem. A* **2007**, *111*, 5582−5592.

(33) Peeters, J.; Nguyen, T. L.; Vereecken, L. *Phys. Chem. Chem. Phys.* **2009**, *11*, 5935−5939.